Internal Flows and Particle Transport Inside Picoliter Droplets of Binary Solvent Mixtures

E.L. Talbot[1], A. Berson[2], L. Yang[1] and C.D. Bain[1]; [1] Department of Chemistry, Durham University, Durham, DH1 3LE, United Kingdom; [2] School of Engineering and Computing Sciences, Durham University, Durham, DH1 3LE, United Kingdom

Abstract

The flows in evaporating droplets of binary mixtures are much more complicated than single solvent systems. Solutal Marangoni flows are generated due to differential evaporation of components. High-speed imaging techniques are used to visualize how internal flows transport particles to build up the end deposit. Circulatory flow along streamlines develops inside droplets at the contact line or central region, depending on the direction of the Marangoni flow. Re-circulation of particles can reduce the build up of a ring stain. Additionally, particles migrate across streamlines to collect at the droplet center independent of where the circulating regions occur. Potential mechanisms for particle migration are discussed, including chemophoresis, thermophoresis and shear-induced migration.

Introduction

In order to predict and control the distribution of particles deposited by a drying droplet, it is necessary to understand how internal flows transport particles during the droplet lifetime. Compared to single solvent droplets with radial flow [1], binary solvent mixtures can develop complex internal flows during drying [2, 3]. Differential evaporation of the components [4, 5] and enhanced evaporation at the periphery [6], results in Marangoni flows which complicate particle transport. Marangoni recirculation cells [7, 8] re-distribute particles, counteracting the build up of the ring stain otherwise seen in droplets with a pinned contact line [9, 10].

In addition to re-distribution by Marangoni flows, other transport mechanisms can affect the deposit. In some cases, particles can migrate across the fluid streamlines [11, 12]. Particle migration can occur along a gradient in the chemical potential [13], along a temperature gradient [14, 15] or due to regional shear rate differences [16].

We explore the effect of the direction, strength and duration of the Marangoni flow on the end deposit using high-speed imaging to follow particle motion. We adjust the relative humidity in order to switch the direction of the Marangoni flow within mixtures of methoxypropanol/water, while keeping the composition constant. The Marangoni strength is determined by the magnitude of the surface tension gradient and controlled by the chemical composition of the mixture. The duration is the period of time the Marangoni flow lasts for, relative to the drying time, and is dependent on the component ratio.

Experimental

Picoliter droplets were generated using a Microfab piezoelectric drop-on-demand device (MJ-ABP-01, Horizon Instruments) with a 50 μm orifice. A high-speed camera (Optronis CR450x3) was used to collect shadowgraph images of the droplet profile from the side. The typical frame rate for side-on acquisition was 500 fps. The volume and contact angle were then extracted using a custom-made MATLAB routine. A spherical cap was assumed, as the droplets had picoliter volumes with corresponding Bond numbers, $Bo \ll 1$.

Simultaneously, an inverted microscope was used in conjunction with a second high-speed camera (Photron APX RS) to track polystyrene tracer particles inside the fluid and to follow the internal flows. Frame rates depended on the mixture composition, but were typically 3000 fps for ethanol/water mixtures and 1000 fps for methoxypropanol/water mixtures. Particle tracking velocimetry (PTV) was carried out to determine the direction of motion and velocities of the particles. The droplets were viewed from below, through the substrate, requiring both the fluid and substrate to be adequately transparent. To this effect glass substrates were used. Glass cover slips fluorinated by plasma treatment of a polybutadiene coating [17] were also suitable for achieving higher contact angles, provided transmitted light levels were high enough to visualize the droplet through the coating.

The binary mixtures used were ethanol/water and methoxypropanol (PM)/water; the surface tensions and vapor pressures are given in table 1. A thermohygrometer (Extech) was used to measure the temperature, T, (typically 20 °C) and relative humidity, RH. A custom-made humidity cell was used to regulate the RH. Typical impact velocities were approximately 1 ms^{-1}.

Table 1. *Surface tensions, σ and vapor pressures, p, at 20°C [18].*

Fluid	σ/ mNm^{-1}	p/ kPa
Ethanol	22.4	5.95
Methoxypropanol	27.0	1.60
Water	72.9	2.34

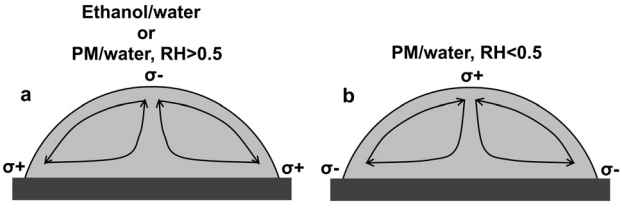

Figure 1. *Theoretical Marangoni flow directions along the liquid-vapor interface in binary mixtures. a) Apex to contact line. b) Contact line to apex.*

The solvents for binary mixtures were chosen to assess

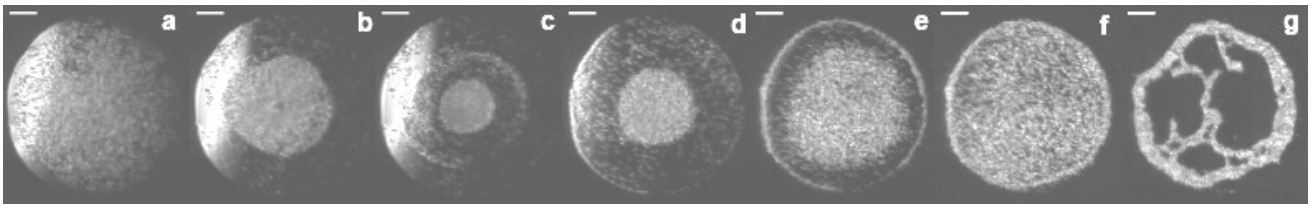

Figure 2. *A droplet of 10%v ethanol/water containing 0.1%v 1-μm polystyrene spheres at a RH of 0.50 on uncoated glass. The group of particles that collects at the droplet center undergoes circulating Marangoni flow. Times normalized by the drying time, t_d, are a) 0.001 t_d, b) 0.05 t_d, c) 0.10 t_d, d) 0.51 t_d, e) 0.82 t_d, f) 0.92 t_d, g) 1.00 t_d. The drying time is 3.27 s. The scale bars are 50 μm*

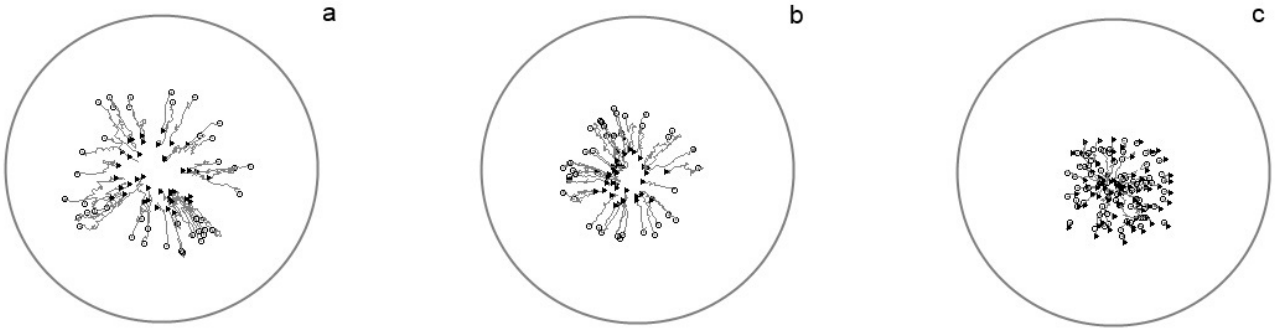

Figure 3. *Particle tracks obtained using PTV for a 50%v ethanol/water droplet containing 0.01%v 1-μm polystyrene spheres on a coated glass substrate at a RH of 0.25. The camera is focused just above the substrate. Particles move inwards from the contact line to the droplet center close to the substrate, consistent with solutal Marangoni flow. A $\circ$ marks the beginning of a track, and a $\triangle$ the end. a) 0.44–0.46 t_d, b) 0.50–0.52 t_d, c 0.53–0.55 t_d. The drying time is 1.65 s, the initial contact diameter is $\backsim$ 200 μm and the initial contact angle is $\backsim 50^{\circ}$.*

the effect of Marangoni flow direction, strength and duration. Marangoni flows are directed along the liquid-vapor interface from low to high surface tension (Fig. 1). There is enhanced evaporation at the contact line compared to the apex of the droplet. Additionally, the more volatile component evaporates preferentially. These two effects combine to increase depletion of the more volatile component at the contact line compared to the apex. Ethanol/water and PM/water (at $RH > 0.5$) have a theoretical Marangoni flow direction from apex to contact line along the liquid-vapor interface (Fig. 1a), as the lower surface tension component is more volatile. PM/water mixtures with a $RH < 0.5$ have the reverse Marangoni flow direction (Fig. 1b). At any RH the ethanol is always more volatile than water. The Marangoni flow direction in the ethanol/water mixtures is always from the apex towards the contact line along the liquid-vapor interface.

The Marangoni flow duration can be altered by changing the ratio of the more volatile component. The strength is determined by the magnitude of the surface tension gradient. The solvents PM and ethanol were chosen as they have similar surface tensions. The surface tension gradient is then influenced by the relative volatility, as a larger difference in vapor pressure causes a larger composition difference from apex to contact line.

Results and Discussion

There were two types of flow seen inside the evaporating droplets of binary mixtures. First, circulating flows driven by surface tension gradients carried particles along the fluid streamlines. Second, particles migrated towards the center of the droplet, across the fluid streamlines. The migratory flow was approximately two orders of magnitude slower than the circulatory flow. The combined effect of the two flows was to form a region of circulatory flow and a quiescent region inside the droplet, with particles gathered at the droplet center. This resulted in a strongly concentrated region of particles at the center of the droplet. The region of concentrated particles had a sharp boundary with a collection radius, R_g, that decreased with time during the period of Marangoni flow. When the Marangoni flow ceased due to depletion of the more volatile solvent, a minimum value of R_g was reached ($R_{g,min}$). There was then radial flow towards the contact line and R_g increased.

To describe the general trends for internal flows in evaporating droplets of binary mixtures, we first look in detail at a droplet of 10%v ethanol/water. The particles were initially uniformly distributed (Fig. 2a). As differential evaporation of the components occurred, surface tension gradients set up Marangoni cells. As the ethanol was depleted, the particles became concentrated at the center of the droplet, leaving a region of fluid near the contact line strongly depleted of particles. The concentrated collection of particles exhibited circulatory motion. $R_{g,min}$ was reached (Fig. 2c) before the internal flow reverted to radial flow towards the contact line (Fig. 2d), building up a ring stain. For this low ethanol concentration, the minimum in R_g occurred early in the evaporation (0.10 t_d). During the last stages of drying (Fig. 2g), capillary forces strongly influenced the morphology of the end deposit, pulling the particles into lacy networked structures within the ring stain.

Figure 3 shows the particle tracks for a droplet with a higher

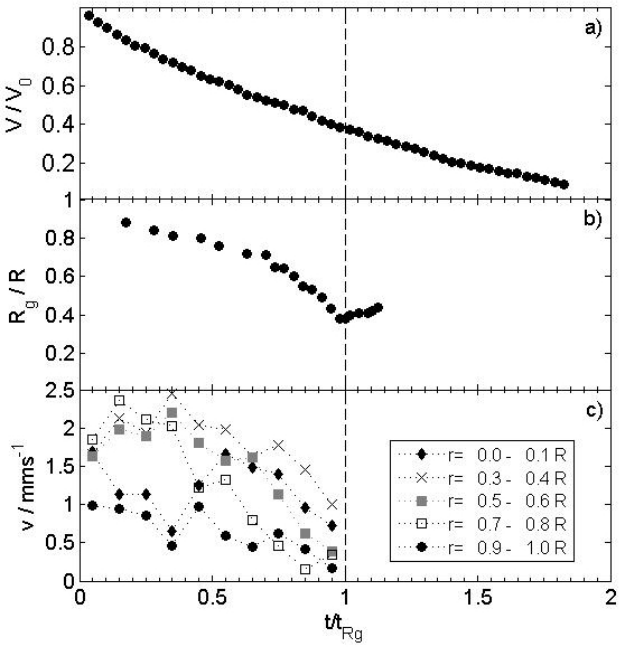

Figure 4. *a) The evaporation rate of a 50%v ethanol/water droplet on uncoated glass, containing 0.01%v 1-μm spheres at a RH of 0.25. b) The evolution of the group radius, R_g, with time, normalized by the initial contact radius, R. t_{Rg} is the time when the transition to radial flow occurs, indicated by the vertical dashed line. c) The mean particle speeds for spatial bins of size $0.1R$. An average is taken for 10 droplets for each spatial bin. The drying time is 1.65 s and the initial contact angle is $\backsim 50^{\circ}$. A typical value for t_{Rg} is 0.9 s.*

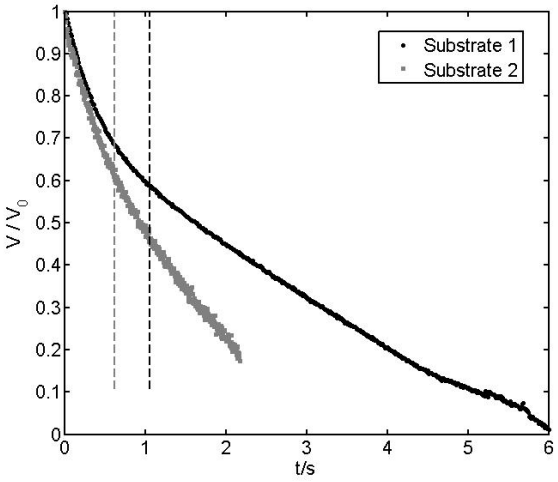

Figure 5. *The evaporation rate of a 50%v ethanol/water droplet containing 0.1%v 1-μm polystyrene spheres on two coated substrates at a RH of 0.5. Substrate 1 has a higher initial contact angle than Substrate 2 (see Fig. 6). Vertical dashed lines indicate when $R_{g,min}$ occurs on each substrate.*

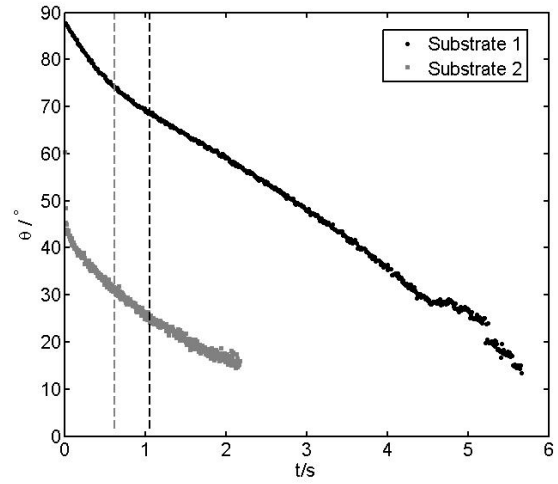

Figure 6. *The contact angle evolution of a 50%v ethanol/water droplet containing 0.1%v 1-μm polystyrene spheres on Substrate 1 (high initial contact angle) and Substrate 2 (lower initial contact angle) at a RH of 0.5. Vertical dashed lines indicate when $R_{g,min}$ occurs on each substrate.*

concentration of ethanol (50%v ethanol/water). A lower concentration of 1-μm polystyrene spheres (0.01%v) allowed the motion of the particles to be resolved. The camera was focused just above the substrate to avoid the no-slip region. Near the substrate, the particles moved from the contact line towards the droplet center, consistent with the expected direction for solutal Marangoni flow (Fig. 1a). Thermal Marangoni flow would have the reverse flow direction (Fig. 1b), due to the longer conduction pathway to the apex. The apex is then colder than the contact line, giving a higher surface tension at the apex of the droplet. The flow direction therefore confirms that solutal Marangoni effects drive the circulating flow rather than thermal gradients.

The particle tracks in Fig. 3 reveal the flow behavior close to the transition from circulatory to radial flow. Before the transition to radial flow, the circulating collection of particles took a toroidal shape, indicated by the central 'hole' seen in Fig. 3a and 3b. This 'hole' was maintained even at dilute particle concentrations and so is not associated with hydrodynamic interactions between particles. As the transition to radial flow was approached, the circulatory motion died out from the contact line inwards (Fig. 3c). The transition from circulatory flow to radial flow was sharp, although particles closer to the contact line moved radially outwards before the inner particles. Finally, all particles flowed radially towards the contact line.

Figure 4a shows the evaporation rate for a 50%v ethanol/water droplet on uncoated glass for a RH of 0.25 calculated from the side profile of the droplet. Figure 4b describes the evolution of the collection radius, R_g, with time. There was an initial decrease in R_g as the particles were restricted to the center of the droplet. The minimum collection radius, $R_{g,min}$, was reached, and radial flow began. The particles were carried towards the contact line and R_g increased. The transition to radial flow was sharp, but figure 4a indicates that this is not associated with a sharp change in the evaporation rate.

The evolution of the particle speed, v, within a 50%v ethanol/water droplet containing 0.01%v 1-μm polystyrene spheres is indicated in Fig. 4c. Dashed lines are meant as a guide

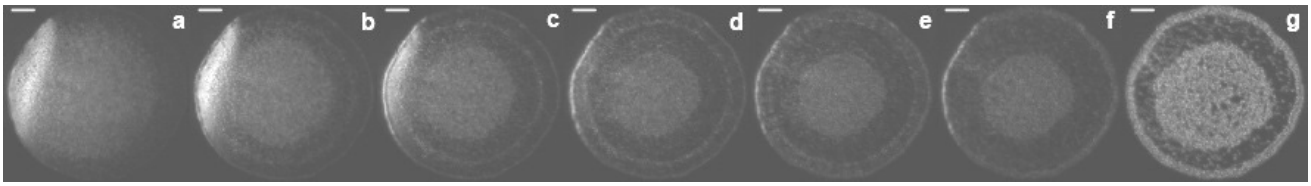

Figure 7. *A droplet of 50%v PM/water containing 0.5%v 600 nm-polystyrene spheres at a RH of 0.50. Circulating flow occurs near the contact line. At the center of the droplet particles migrate inwards, but there is no circulatory flow. A depletion zone exists between these two flow regimes. Times normalized by the drying time, t_d, are a) 0.08 t_d, b) 0.23 t_d, c) 0.38 t_d, d) 0.54 t_d, e) 0.69 t_d, f) 0.85 t_d, g) 1.00 t_d. The scale bars are 50 µm.*

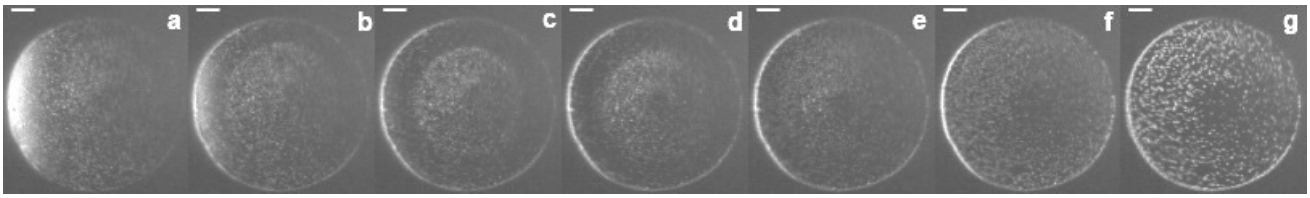

Figure 8. *A droplet of 50%v PM/water containing 0.1%v 600 nm-polystyrene spheres at a RH of 0.65. Two regions of flow are apparent as drying progresses. An inner region of circulating flow and an outer region of radial flow. Times normalized by the drying time, t_d, are a) 0.15 t_d, b) 0.30 t_d, c) 0.44 t_d, d) 0.58 t_d, e) 0.73 t_d, f) 0.88 t_d, g) 1.00 t_d. The scale bars are 50 µm*

to the eye. Particle speeds were binned spatially in increments of $0.1R$, where R is the droplet radius, and in temporal bins of $0.1t_{Rg}$, where t_{Rg} is the time at which the transition to radial flow occurred. The average speeds within each bin were then plotted at the mid-point of the temporal bin. The mean speed in the x-y plane was used and not the radial speed, as the vortex was not always at the droplet center. Brownian motion did not strongly influence the mean speeds. There was a gradual drop in the mean particle speed near the droplet center from ~ 1.8 mms^{-1} at early times to ~ 1 mms^{-1} close to the transition time, t_{Rg}. At early times the mean speed was $\backsim 2$ mms^{-1} everywhere except close to the contact line (0.9–$1.0R$), where the mean speeds were much slower (~ 1 mms^{-1}).

Figures 5 and 6 indicate where the minimum radius of the collected particle group, $R_{g,min}$, occurred for a 50%v ethanol/water droplet relative to the evaporation rate and contact angle at a *RH* of 0.5 on two coated substrates. The chemical composition of the substrates is the same, but the surface roughness differs. The rougher surface of Substrate 1 leads to higher contact angles. The transition from circulatory flow to radial flow, which occurs after $R_{g,min}$ is reached, corresponds to the same normalized volume loss on each substrate (Fig. 5). There is no dependence on the contact angle (Fig. 6). It is therefore a particular chemical composition (at fixed *RH*) that is important in determining when $R_{g,min}$ occurs, at least for these two initial contact angles.

To investigate the effect of the Marangoni flow direction on internal flows, we compare droplets of PM/water of the same initial composition (50%*v* PM/water) at different relative humidity, *RH*. For a *RH* below approximately 0.5, the water evaporated faster than the PM. At a *RH* above about 0.5, the relative volatility of the water and PM was reversed, switching the Marangoni flow direction (Fig. 1b). Figure 7 shows a sequence of images for a drying droplet of 50%*v* PM/water at a *RH* of 0.50 where water evaporated faster than PM. Initially, particles were uniformly dispersed throughout the droplet (Fig. 7a). Solutal Marangoni flow resulted from a gradient in the chemical composition along the liquid-vapor interface. In this case, the direction of the circulatory Marangoni flow (observed using PTV) was from the contact line towards the apex along the liquid-vapor interface. The circulating region was observed near the contact line with a quiescent region at the droplet center. As time progressed, particles concentrated in the center and in the circulating region near the contact line. In between was a region depleted of particles. There was no circulatory motion of particles located at the droplet center.

For a drying droplet of 50%*v* PM/water at a *RH* of 0.65 (Fig. 8) , circulatory flow occurred at the droplet center, while near the contact line, flow was slower and radially outwards. Similar to the same mixture at lower *RH* (Fig. 7), particles gathered at the droplet center, but in this case circulating flow within the group kept particles moving. Particles collected at the center of droplets for both high and low *RH*, independent of where the circulatory region of flow was within the droplet. This observation suggests that the direction of the Marangoni flow along the liquid-vapor interface is important for determining where the regions of circulatory and quiescent flow occur, but not for the migration of particles to the center of the droplet. As the direction of flow depends on whether the more volatile component has the highest surface tension, the flow regimes were dependent on whether the surface tension gradient increased or decreased during drying. If the more volatile component, e.g. ethanol, had the lower surface tension, the surface tension gradient increased with time on depletion as the surface tension changes more steeply with composition at low ethanol content.

To explore the effect of the strength of the Marangoni flow on particle transport, two solvents with a large difference in vapor pressure (ethanol/water) were compared with a solvent pair of similar vapor pressure (PM/water). The surface tensions of ethanol and PM are similar. The compositional gradient should be enhanced in ethanol/water by a larger vapor pressure difference, increasing the Marangoni forces. In an ethanol/water

droplet, the region near the contact line became significantly more depleted of particles than in the PM/water mixture, with fewer particles escaping the central collection (Fig. 2). Most of the particles collected at the droplet center with a smaller $R_{g,min}$ than for the PM/water mixtures. The direction of the Marangoni flow in ethanol/water mixtures was confirmed by PTV to be along the liquid-vapor interface from apex to contact line. The direction was the same as for PM/water at high RH (> 0.5) and similarly the region of circulating flow was near the center of the droplet. The Marangoni strength influenced the size of $R_{g,min}$ and the extent of particle depletion.

The effect of Marangoni flow strength was confirmed using ethanol/water mixtures and varying the ethanol content. R_g was dependent on the concentration of ethanol inside the droplet. For droplets with ethanol concentrations between 10-50%v, the collection was strong forming a smaller $R_{g,min}$. Above 50%v ethanol content, particle collection was weaker. Surface tension gradients increased at lower ethanol concentrations. Additionally, circulating velocities were larger inside droplets with lower initial ethanol concentrations. Both factors could influence the size of the collected group.

The influence of the duration of the Marangoni flow was assessed using ethanol/water mixtures of ethanol content between 10–90%v. Ring stains were suppressed during the initial Marangoni phase of drying (Fig. 2a-c) for all the mixtures studied. After the Marangoni phase of drying, internal flows carried particles radially outwards as with single solvent droplets. During this second phase of radial flow, a ring stain began to build up (Fig. 2e). The duration of the Marangoni flow therefore influences the time available for ring stain build-up. However, the Marangoni duration also determines the volume of liquid lost via evaporation before the transition to radial flow. A larger volume loss increases the solid content at the transition to radial flow. For a pure solvent, a higher solid volume fraction results in a wider ring. As lower ethanol content resulted in thinner ring stains, we suggest there is a competing effect between the degree of collection (stronger at low ethanol content), the period of central collection and the solid content at the transition. Marangoni flow did not fully suppress the ring stain for PM/water mixtures, although the ring stain grew more slowly while the Marangoni circulation persisted.

Particles migrated across fluid streamlines to collect at the center of the droplets. Potential mechanisms for the migration include chemophoresis, thermophoresis (the Soret effect) and shear-induced migration. First we consider chemophoresis. For migration to be solely chemophoretic, particle motion would be towards a preferred solvent. If this were the case, we would expect to see a switch in the direction of migration in PM/water mixtures on increasing the RH above 0.5, which is not observed experimentally. The migration cannot be due to a chemical potential gradient alone. It is however possible that chemophoresis could be a contributing mechanism, as we have seen from the circulatory flows that solutal gradients are significant in these mixtures.

Second, we consider thermophoresis. Droplets were deposited onto glass with a low thermal conductivity ($1\ Wm^{-1}K^{-1}$) and also onto sapphire with a higher thermal conductivity ($35\ Wm^{-1}K^{-1}$). Evaporative cooling is enhanced on substrates with low thermal conductivity [19]. Therefore, a reduction in particle migration or no migration at all, was expected on sapphire for a thermophoretic mechanism. However, particle collection was the same on each substrate. Also, water droplets showed only radial flow indicating that thermal effects due to evaporative cooling were not present. At RH values below $\backsim 0.5$, PM evaporates more slowly than water. Consequently, no thermal effects are expected in these mixtures but particle collection still occurred (Fig. 7). Additionally, PTV indicated that the direction of the Marangoni flow was from apex to contact line along the liquid-vapor interface when the lower surface tension component was evaporating fastest. This is consistent with solutal Marangoni flow, whereas thermal Marangoni flow would occur in the reverse direction. We can therefore rule out thermophoresis as the migration mechanism.

Last, we look at shear-induced migration. Potential causes for shear-induced migration include an asymmetric collision distribution [16] or lift on the spheres [20]. Migration for these mechanisms is from regions of high shear rate to regions of low shear rate. The observed velocities in our droplets of 50%v ethanol/water are approximately 2.5 mms^{-1}. The corresponding shear rate, $\dot{\gamma}$, inside a droplet of 50%v ethanol/water with a height of $\sim 30\ \mu$m is $\dot{\gamma} \sim u/H \sim 2\ \text{mms}^{-1}$ / $30\ \mu\text{m} \sim 70\ \text{s}^{-1}$. The particle Reynolds number in our 50%v ethanol/water droplets can be defined as $Re \backsim \rho_f a^2 \dot{\gamma}/\mu_f \backsim 995\ \text{kgm}^{-3} \times (1\ \mu\text{m})^2 \times 70\ \text{s}^{-1}$ / 0.89 mPas $\backsim 10^{-5}$, with $a\dot{\gamma}$ the change in shear rate over the length-scale of the particle. ρ_f is the fluid density, μ_f is the fluid viscosity and a is the particle radius. Shear induced migration in a capillary at lower Reynolds number (10^{-6}) has previously been observed by Brown et al. [16] at lower shear rates (below $10\ \text{s}^{-1}$). We also note a size-dependence to the particle collection, with larger particles migrating to the droplet center faster than small particles. This is consistent with previous observations for shear-induced migration by Semwogerere and Weeks [11]. The size of the droplet is important for determining the extent of collection as well as the particle size. We did not observe particle collection in microliter droplets, although circulatory motion occurred. Microliter droplets have lower shear rates which could explain the lack of collection. Finally, the toroidal shape of the particle collection is consisitent with migration towards the low shear rate regions of Marangoni cells.

Conclusion

To summarize, Marangoni flows occurred inside droplets of binary mixtures, due to surface tension gradients resulting from differential evaporation of the solvents. Particles within droplets undergoing Marangoni flow migrated towards the center of the droplet as evaporation progressed. When the Marangoni flow period ended, particles moved radially outward towards the contact line. The duration and strength of the Marangoni flow determined how many particles escaped the central collection to form a ring stain. Additionally, a stronger Marangoni flow caused a smaller radius of the collected central group. The direction of the Marangoni flow influenced the circulatory flow regimes seen inside the evaporating droplets from particle motion along fluid streamlines. The concentrated particle collection at the center of picoliter droplets resulted from particle migration across the fluid streamlines. The migration was towards the droplet center independent of the Marangoni flow direction. A potential migra-

tion mechanism is shear-induced migration, though chemophoresis could contribute. Capillary forces during the last stages of drying played a key role in the morphology of the end deposit.

Acknowledgments

The authors thank P.S. Brown (Durham University) for fabricating the plasma fluorinated substrates, and H.N. Yow (Leeds University) for the polystyrene spheres. This work was financed by EPSRC (grant number EP/H018913/1).

References

[1] R.D. Deegan, O. Bakajin, T.F. Dupont, G. Huber, S.R. Nagel and T.A. Witten, Nature **389**, 6653, 827–829 (1997).
[2] Y. Hamamoto, J.R.E. Christy and K. Sefiane, J. Thermal Sci. Technol. **7**, 3, 425–436 (2012).
[3] I. Ueno and K. Kochiya, Adv. Space Res. **41**, 12, 2089–2093 (2008).
[4] A.K.H. Cheng, D.M. Soolaman and H-Z. Yu, J. Phys. Chem. B **110**, 23, 11267–11271 (2006).
[5] K. Sefiane, S. David and E.R. Shanahan, J. Phys. Chem. B **112**, 36, 11317–11323 (2008).
[6] R.D. Deegan, O. Bakajin, T.F. Dupont, G. Huber, S.R. Nagel and T.A. Witten, Phys. Rev. E **62**, 1, 756–765 (2000).
[7] H. Hu and R.G. Larson, Langmuir **21**, 9, 3972–3980 (2005).
[8] H. Hu and R.G. Larson, J. Phys. Chem. B **110**, 14, 7090–7094 (2006).
[9] J. Park and J. Moon, Langmuir **22**, 8, 3506–3513 (2006).
[10] T. Still, P.J. Junker and A.G. Yodh, Langmuir **28**, 11, 4984-4988 (2012).
[11] D. Semwogerere and E.R. Weeks, Phys. Fluids **20**, 043306 (2008).
[12] A. Ramachandran and D.T. Leighton Jr., J. Fluid Mech. **603**, 207–243 (2008).
[13] A. Kabalnov and H. Wennerstrom, Soft Matter **5**, 23, 4712–4718 (2009).
[14] R. Kita, G. Kircher and S. Wiegand, J. Chem. Phys. **121**, 18, 9140–9146 (2004).
[15] S. Iacopini, R. Rusconi and R. Piazza, Eur. Phys. J. E **19**, 1, 56–67 (2006).
[16] J.R. Brown, E.O. Fridjonsson, J.D. Seymour and S.L. Codd, Phys. Fluids **21**, 093301 (2009).
[17] I. Woodward, W. C. E. Schofield, V. Roucoules and J. P. S. Badyal, Langmuir **19**, 3432 (2003).
[18] Lange's Handbook of Chemistry 15th Edition, McGraw Hill (1999).
[19] E.L. Talbot, A. Berson, P.S. Brown and C.D. Bain, Phys. Rev. E **85**, 061604 (2012).
[20] J.B. McLaughlin, J. Fluid Mech. **224**, 261–274 (1991).

Author Biography

Emma Talbot received her MSci Joint Honors in Chemistry and Physics from the University of Durham, UK in 2010. She remained at the University of Durham, and is in the final year of her PhD in chemistry supervised by Prof. C.D. Bain.